Chapter

Interference Mapping in 3D for High-Density Indoor IoT Deployments

Antoni Ivanov, Viktor Stoynov, Kliment Angelov, Radostin Stefanov, Dimitar Atamyan, Krasimir Tonchev and Vladimir Poulkov

Abstract

Deployment of practical Internet of Things (IoT) in the context of 5G can be hindered by substantial interference and spectrum limitations, especially in the unlicensed frequency bands. Due to the high density of such devices in indoor scenarios, the need for interference characterization which facilitates more effective spectrum utilization is further emphasized. This chapter studies the influence of diverse scenarios for the dense placement of interferers on the spectrum occupancy through the use of 3D interference maps for two popular IoT technologies—LoRa and Wi-Fi. The experiments are performed with software-defined radio (SDR) platforms in real time and an automated positioning tool which provides the measurements to characterize the interference in 3D space. The findings demonstrate a nonuniform character of the interference and the significant impact of fading within the width, height, and length of the examined area. They suggest the role of dynamic relocation for realistic IoT scenarios.

Keywords: 3D interference maps, Internet of Things, sensors, deployment density, spectrum utilization, ultra-dense networks

1. Introduction

Traditional wireless technologies (such as cellular networks) have very limited or no practicality for providing wide area and low-powered communications due to their intensive signal processing and device output power requirements, which would lead to unacceptable energy consumption for the case of Internet of Things (IoT) scenarios. This is the main consideration behind the development of the low-powered wide area network (LPWAN) communication standards such as Sigfox, ZigBee, LoRa, Wi-Fi, etc. Modern IoT technologies show a great potential in the development of agile solutions to novel applications (such as intelligent metering, automated industrial production, home security, and eHealth), which will expand the wireless communications' scope well beyond connected computers, smartphones, and tablets to incorporate a wide range of intelligent appliances and specialized equipment in many areas of human personal and professional life. A recent example is the recognition of the potency of IoT-empowered health care for

the efficient treatment of patients, identification of infection clusters, and disease spread prevention during the current, unprecedented COIVD-19 situation [1]. Furthermore, it has been estimated that the number of connected devices is already several times higher than the world's current population [2] and the majority of them will be established through widespread standards such as Wi-Fi, with others such as LoRa also gaining prominence [3]. Despite the technological advances and the variety of technologies and modulation types used, there are a number of challenges that can complicate the operation of the IoT devices running in the Industrial, Scientific, and Medical (ISM) band.

1. Harmonization of ISM bands: in practice, IoT applications are being deployed both in the 868 MHz and 2.4 GHz bands and in those that are not regulated. The ISM range varies for international or national use and it is not harmonized, which may lead to complex interference scenarios [4].

2. Increased demand for radio-frequency spectrum: with increasing number of devices running in ISM bands, the need to provide more operating frequency bands also increases. However, due to the limited availability of free bands, finding free spectrum is a serious challenge. The application of solutions based on cognitive radio and the operation in occupied ISM or unlicensed frequency bands can help meet the growing demand for spectral bands. In this way, the available frequency bands can be used more efficiently and economically.

3. Mutual interference: coexistence of multiple IoT devices in one ISM heterogeneous environment with similar technical specification can cause significant mutual interference. The application of interference coordination approaches can solve this problem. Applying ISM band-specific interference reduction methods can facilitate the harmonious functioning of different heterogeneous ISM devices [5].

The 2.45 GHz ISM band is also interesting because of the ability to flexibly access the radio spectrum, and through the use of cognitive radio methods, problems of interaction between collaborative systems can be avoided. Due to the potential of this ISM band, many cognitive test beds have been developed. There are already many unlicensed devices that use the spectrum in this band in an intelligent manner. But when the spectrum is saturated with more devices, this will result in interference occurrence. In order to assess the feasibility of applying cognitive methods for the use of spectrum, it is necessary to estimate the occupancy in the ISM bands by using long-term monitoring. Due to the huge number of different devices and applications, operating especially in the 2.45 GHz band, differences in the usage of the spectra can be significant and vary considerably even in a small area.

The ever-increasing attractiveness of LPWANs in industrial and research communities is mainly caused by their low energy consumption, low-cost communication characteristics, and long-range communication capabilities. Normally, these networks are able to offer coverage within 10–40 km in rural zones and 1–5 km in urban zones [6]. Furthermore, the LPWANs are tremendously energy efficient, with up to 10 or more years of battery lifetime, and low cost, at around the cost of a single radio chipset [7]. In this context, the features and capabilities of LPWANs have stimulated engineers to realize numerous experimental studies on their performance in outdoor and indoor environments. The up-to-date LPWAN technologies usually use gateways, referred to as concentrators or base stations (BSs), to serve end devices. In this context, the end devices communicate directly with one or more gateways. This is the major difference between traditional WSNs and LPWANs. This type of topology

meaningfully simplifies the coverage of large regions, even spanning an entire nation, by taking advantage of the already deployed cellular network infrastructure. Thus, the experiments presented in this chapter are focused on LoRa and Wi-Fi for IoT.

LoRa wide area networks (WANs) are a low-power specification for IoT devices operating in the regional, national, or global networks. It is frequency-agnostic and can use the 433, 868, or 915 MHz bands in the Industrial, Scientific, and Medical (ISM) range, depending on the region in which it is located. LoRa is the physical layer or wireless modulation that is used to implement a long-distance communication link. Data transmission speeds vary from 0.3 to 50 kbps, depending on whether channel aggregation is used. The standard LoRa operates in the 868 MHz (EU)/915 MHz (US) frequency range at a distance of 2–5 km (urban environment) and up to 15 km (suburban), with a transmission speed not higher than 50 kbps. The advantage of the technology is the ability to achieve long-distance connections, with a single base station having the capability to cover hundreds of square kilometers. The size of the covered range is highly dependent on the environment and the presence of obstacles, but LoRaWANs have the best power supply organization when compared to any other standardized communication technology [8].

LoRaWANs employ bidirectional communication by means of a special chirp spread spectrum (CSS) modulation technique, in this way, distributing a narrow band input signal over an expanded channel bandwidth. The signal which results has properties which resemble those of noise, rendering detecting or jamming more difficult. The CSS processing allows increased resistance to both noise and interference [9]. By the same token, however, other technologies operating in the same ISM band may themselves generate interference. Many LoRa parameters such as carrier frequency (CF), spreading factor (SF), bandwidth (BW) and CR can be tuned in order to optimize the performance. The challenges before the implementation of LoRa are related to the implementation of the cognitive network concept, densification and technology coexistence, and interoperability. The maximum duty cycle of devices operating in the ISM bands has a significant influence on the capacity of the network. One of the more important future directions is the integration of cognitive radio into the LoRa standard. In the future, the addition of cognitive radio into the LoRa standard would result in a meaningful reduction in energy consumption. The practical implementation of LPWAN technologies, and exceptionally LoRaWANs, poses challenges for coexistence as the employment of gateways increases in urban regions. It is essential to devise coordination mechanisms between gateways from the same or different operators to limit interference and collisions. The coexistence mechanisms include coordination and reconfiguration protocols for gateways and end devices. The high attractiveness of LPWANs gives rise to a new challenge called technology coexistence. Many autonomous networks will be implemented in close proximity and the interference between them must be controlled in order to keep them in operational state. Nowadays, LPWANs are not designed to handle this forthcoming challenge that will cause the spectrum becoming overly crowded. Coexistence management for Wi-Fi and Bluetooth will not operate well in the context of LPWANs' deployment. Due to their large coverage areas, LPWAN devices can be subject to an exceptional number of hidden terminals. Enabling different technologies to coexist on the same spectrum is very challenging, mainly due to different entities maintaining different technologies [10].

There are a number of IoT usage scenarios and solutions which utilize the Wi-Fi standard. User identification and authentication is important for robust access to smart home appliances and specific usage data collection and processing (for example eHealth monitoring and access control to various appliances depending on the physiological and behavioral traits of the different members of the household) [11]. Using Deep Learning, this can be achieved without separate dedicated devices

via the channel state information (CSI) extracted from the Wi-Fi signals that are transmitted by the IoT devices during their operation as they are reflected in different manners from users of diverse categories (defined by their age, body shape, and daily routine). Interoperability between Wi-Fi-based IoT and other widespread wireless standards is another significant issue in literature. For example, in agricultural automation, these devices have to operate together with Bluetooth and radio-frequency identification (RFID) instruments. Their coexistence in the Industrial, Scientific, and Medical (ISM) band can be facilitated via rigorous analysis and adaptive frequency hopping [12]. Another aspect of interoperability is addressed for the case of operation between IoT and traditional wireless devices within the 2.4 GHz band due to the different characters of their dataflows. The IoT appliances with their acute battery limitations require low-latency and energy-efficient communications which may be complicated by the bandwidth-intensive transmissions of computers and smartphones. A solution to this issue is implementing an adaptive admission control for the IoT flows, which considers the wireless channel's characteristics [13]. Alternatively, this kind of interoperability is addressed via a Wi-Fi physical layer modification which utilizes multi-antenna access point (AP) [14] or traffic differentiation between IoT and traditional communications through advanced packet scheduling [15].

Scientific efforts are made to solve the present and future issues (mainly in terms to their dependability [16, 17]) with their practical deployment in 5G and beyond networks. Many of them have been focused on multiple wireless standards' coexistence in the license-free spectrum [18], interference mitigation, and coverage extension in the urban environment from the point of view of the overall access networks [6, 19, 20] or controlled retransmission of messages to increase the QoS by avoiding collisions [21]. Such approaches will need to be supplemented by a characterization of spectrum usage, which facilitates utilization analysis and implementation of dynamic access to the shared frequency resource via cognitive radio (CR)-enabled devices. In the ISM bands which are already heavily congested by traditional communications, the necessity of such software-defined monitoring is even more present. Furthermore, spectrum utilization is very different in indoor and outdoor scenarios, which requires that they should be analyzed separately [22]. Based on these observations, the importance of IoT's interoperability in indoor environments is established, and thus, the necessity for interference analysis is emphasized.

The experiments presented in this chapter examine and evaluate the spectrum occupancy and interference of dense indoor scenario for LoRa and Wi-Fi. Multiple interferers for each of these two standards are implemented using the hardware platform PlutoSDR by Analog Devices to develop the high deployment density scenarios expected in 5G, where substantial levels of mutual interference are almost inevitable. Their influence on the spectrum occupancy is shown through 3D interference maps built using an automated testbench, which collects the received signal strength measurements at each location in the examined area for six deployment scenarios in which the number of active interferers and the density of their placement are varied. Thus, this chapter presents the following contributions:

- 3D heatmaps for different deployment densities and locations of interferers in LoRa and Wi-Fi standards.

- Exemplifies the limitation of IoT devices' density and interference avoidance as the number of interferers increases.

- Exemplifies the effect of fading for localization of interference-free areas.

The rest of this chapter is organized as follows. Section 2 describes the experimental setup, the measurement collection system, the hardware and software tools used, and the procedure for data processing. Section 3 illustrates the results, while the conclusions and directions for future work are given in Section 4.

2. Experimental scenarios and data processing

2.1 Experimental setup

The setup for the experiments is shown in **Figure 1**, and it encompasses an area with dimensions of [6000 x 2000 x 800] mm, which is the scope of coverage of the automated positioning system (APS). The APS utilizes a mechanical automated positioning tool (APT, marked with a yellow rectangle in **Figure 2**), which moves along a route preliminary programmed via the computer operating the APS. This route is within the width, length, and height of the aforementioned dimensions, that is, restricted by the four columns, as shown in **Figure 2**. A laptop computer controlling the PlutoSDR receiver which collects the measurements is mounted on the APT (**Figure 1**). The APS covers a plane with dimensions of [6000 x 2000] mm at each of these four elevation levels—0, 250, 500, and 750 mm. They form the 3D axis along which the APT moves. The 3D interference map is produced from the measurements by cubic interpolation.

Four PlutoSDR transmitters which play the role of interferers for other potential IoT nodes in both the LoRa and Wi-Fi standards are shown in **Figures 1** and **2**. They are placed at the four corners of the area's periphery (**Figure 1**; they are also marked with red rectangles in **Figure 2**). Thus, six scenarios for the interferers' density and spectrum occupancy are formed for each of the two wireless standards. Their description is outlined in **Table 1**. In the first four scenarios, the interferers are placed in the periphery, 2 m from the edge of the table which is situated in the middle of the experimental setup. In each of these scenarios, the spectrum occupancy is assessed depending on the number of active interferers. For the other two, all four transmitters are active but they are moved closer to the table—by 1 m for the middle position (S5) and by 2 m, that is, the interferers are placed on the four edges of the table for closest positions (S6).

All interferers have a transmission power of −3 dBm (PlutoSDR has an output power of 7 dBm and a 10 dB attenuation setting is applied [23]). The transmitters as well as the receivers are implemented using the GNU Radio software package [24], while the periods of transmission, reception, and measurement are managed via a Python script. The operational parameters of the SDR nodes are described in **Table 2**.

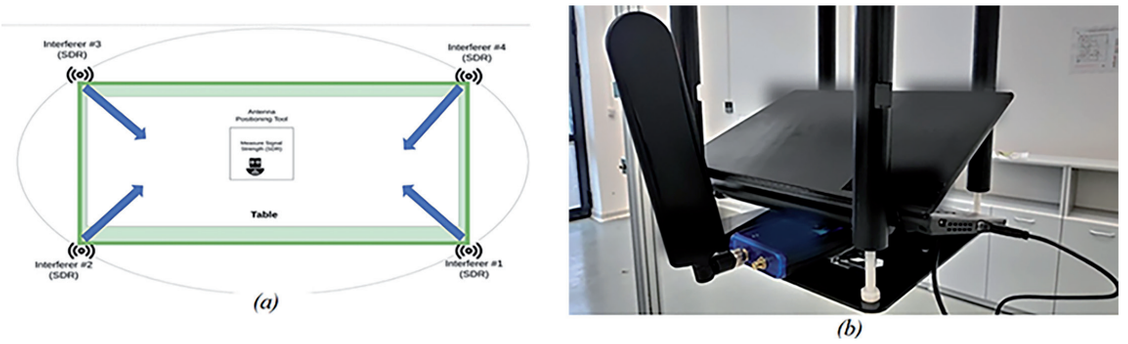

Figure 1.
Experimental setup and APT with (a) PlutoSDR and (b) its host computer.

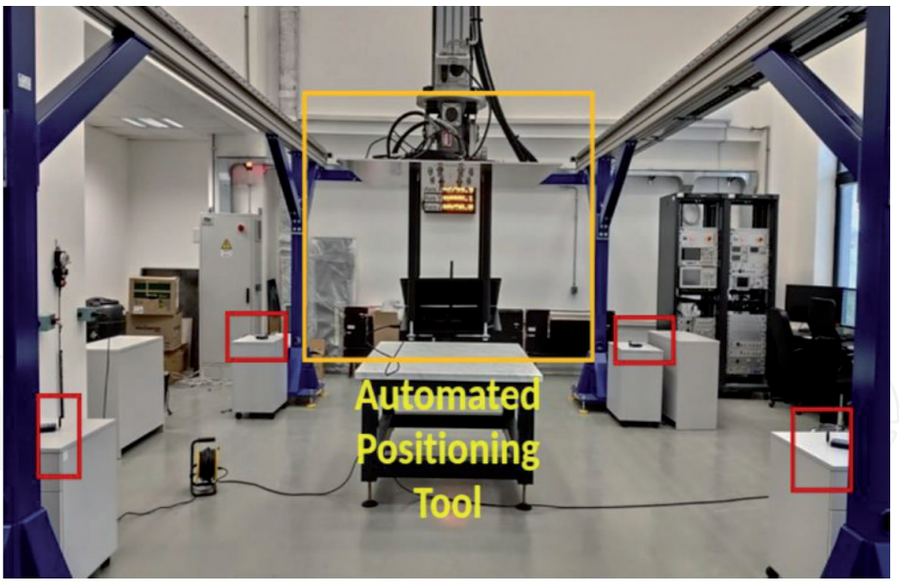

Figure 2.
APS and APT.

	Scenario description	Active transmitters
S1	One interferer	#1
S2	Two interferers	#1 and #3
S3	Three interferers	#1, #2, and #3
S4	Four interferers (farthest position)	#1, #2, #3, and #4
S5	Four interferers (middle position)	#1, #2, #3, and #4
S6	Four interferers (closest position)	#1, #2, #3, and #4

Table 1.
Deployment scenarios.

Parameter	Value
Center frequency	868 MHz (LoRa)/2.484 GHz (Wi-Fi)
Bandwidth	125 kHz (LoRa)/5 MHz (Wi-Fi)
Antenna gain	2 dBi (LoRa)/4 dBi (Wi-Fi)
Transmission power	−3 dBm

Table 2.
Operational parameters.

The APS collects the measurement samples by moving along the [6000 x 2000] mm plane for each of the four heights with a step of 1000 mm in the x-coordinate (i.e., the length) and 200 mm in the y-coordinate (width), as underlined in **Figure 3**. As a result, each plane contains 77 measuring points (marked with ×). At each point, the APS performs one measurement over a period of 7 s. After covering all points of the current plane, the APT is elevated by 250 mm and the process is repeated for each of the four heights (0, 250, 500, and 750 mm in the z-coordinate).

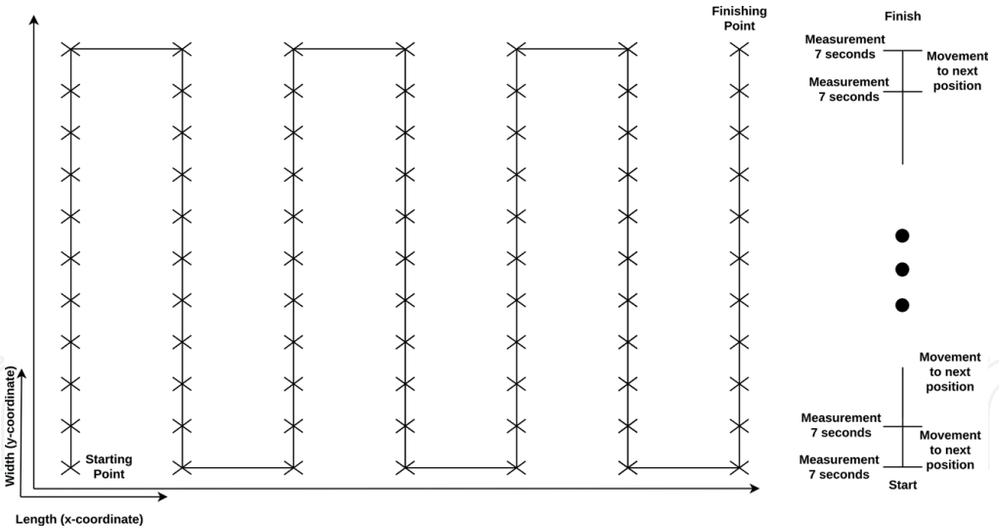

Figure 3.
A schematic of the measurement path for a single plane.

2.2 Data processing

To construct the 3D interference maps, the measured signal batches at each measurement point need to be filtered out so that only the samples with the strongest amplitude remain. Thus, their mean which characterizes the signal strength at this point will be maximized. The filtering is performed on the basis of energy detection spectrum sensing in the following way. For each 256 samples in the signal batch, their mean is compared against a constant decision threshold that is predetermined based on the highest instantaneous amplitude shown in the time domain representation of the batch. The higher the threshold's value is, the fewer samples will be produced in the resulting signal after the filtration. A minimal number of samples is chosen (at least a few hundred, usually in CR studies, over a few thousand [25], 30,000 in this case). If the threshold is too high for at least that number of samples to be produced, it is lowered by 2.5%. This coefficient is determined empirically as a viable compromise between the resulting number of samples and the speed of the process (a smaller reduction decreases the speed but will lead to limiting the signal samples to those which will amount to the highest mean).

3. 3D interference maps

The mean value of the filtered signal determines the power of the received interference power at each measurement point. In each of the six scenarios, a 3D interference map is constructed for both the Wi-Fi and LoRa standards via cubic interpolation of the received interference power means of the 77 measurement points at each of the four elevation levels (0, 250, 500, and 750 mm) in a separate plane. These planes describe the 2D interference distributions (illustrated with the color map) at each height, while together they represent the interference in 3D.

The interference maps for LoRa and Wi-Fi for the six scenarios are illustrated in **Figures 4–13**. To examine more closely some sections of the maps' layers which are partly obstructed by higher planes (i.e., the y-coordinate interval of [0; 1000] mm), they are represented as 3D bar plots. Such graphics are included for Scenarios **S1** and **S6** for LoRa (**Figures 5** and **8**) and **S3** and **S5** for Wi-Fi (**Figures 11** and **13**)

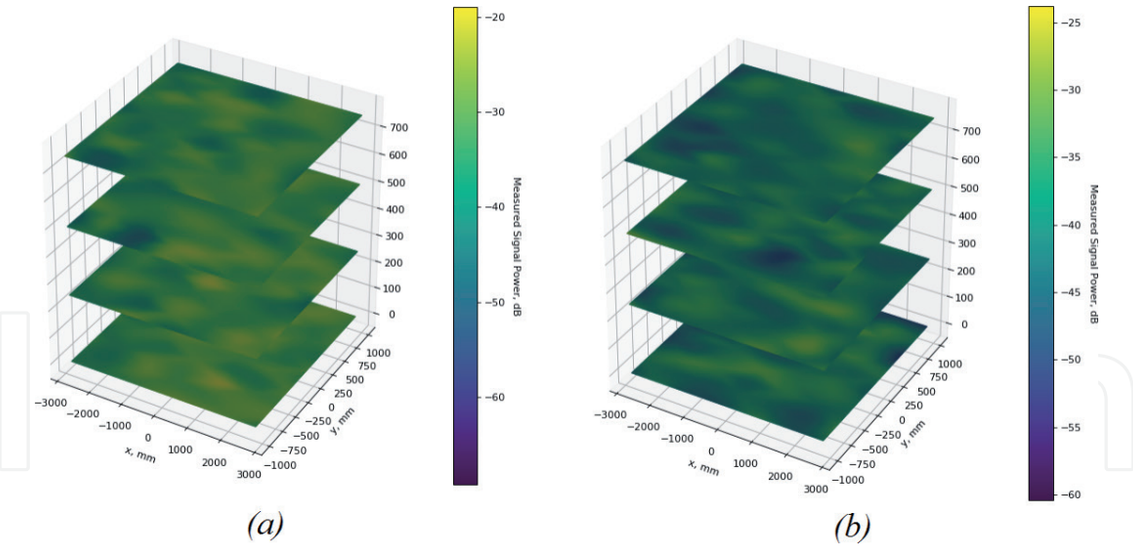

Figure 4.
3D interference map for (a) 868 MHz (LoRa) and (b) 2.484 GHz (Wi-Fi) for z = [0, 250, 500, 750], scenario **S1** *(one active transmitter).*

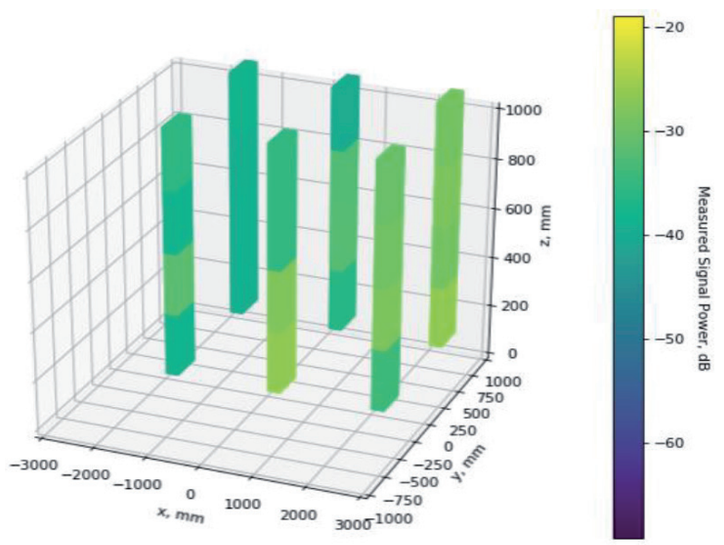

Figure 5.
3D bar plot for the LoRa sensor, z = [0, 250, 500, 750] and x = [−2000, −0, 2000], Scenario **S1**.

because they provide significant information for weak-signal spots which are not clearly seen in the complete 3D interference maps. **Table 3** outlines the coordinates (in x- and y-axes) at which the signal power bars are shown.

Starting with the first four scenarios, the spectrum occupancy is examined with the increase of the number of transmitters. For LoRa, it is clear that a significant portion of the area is permeated with strong signals even for a single active interferer. There is, however, some dissipation with height which creates sections with low interference power (spectrum holes) where communication may be feasible, especially on the opposite end of the area as seen from **Figure 5**. They are also present, even though much more limited, for the second scenario (**Figure 6**) and are localized away from the active interferers (#1 and #3, situated on bottom-right and top-left corners of **Figure 1**, respectively). As the number of emitters is increased, sections with very high interference power are only broadened (**Figures 7** and **9**).

For the other two scenarios which bring the four active interferers closer to each other (**Figures 10** and **12**), no significant difference in the power intensity is observed. Nevertheless, the sections with the highest interference concentration

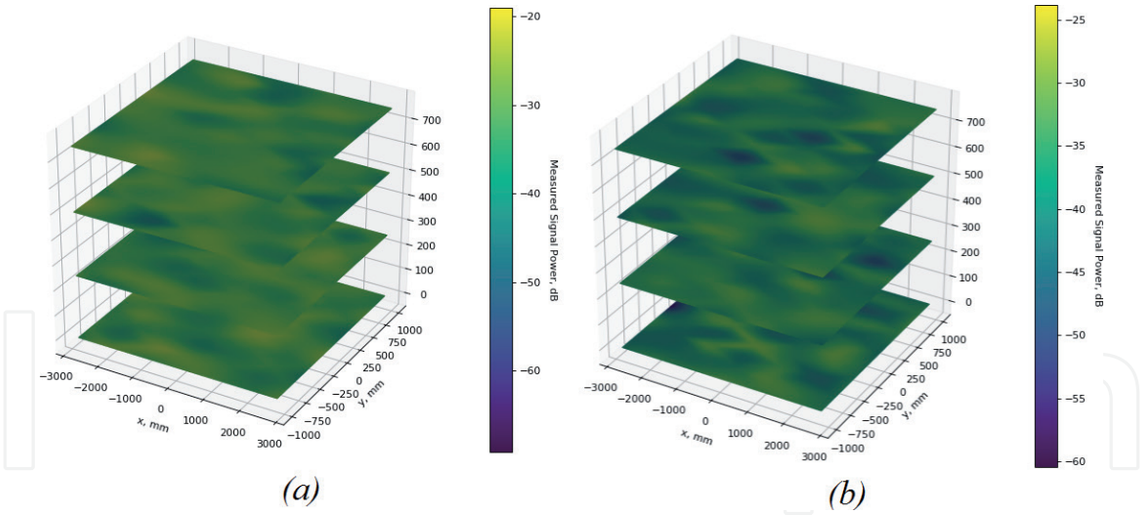

Figure 6.
3D interference map for (a) 868 MHz (LoRa) and (b) 2.484 GHz (Wi-Fi) for z = [0, 250, 500, 750], scenario **S2** *(two active transmitters).*

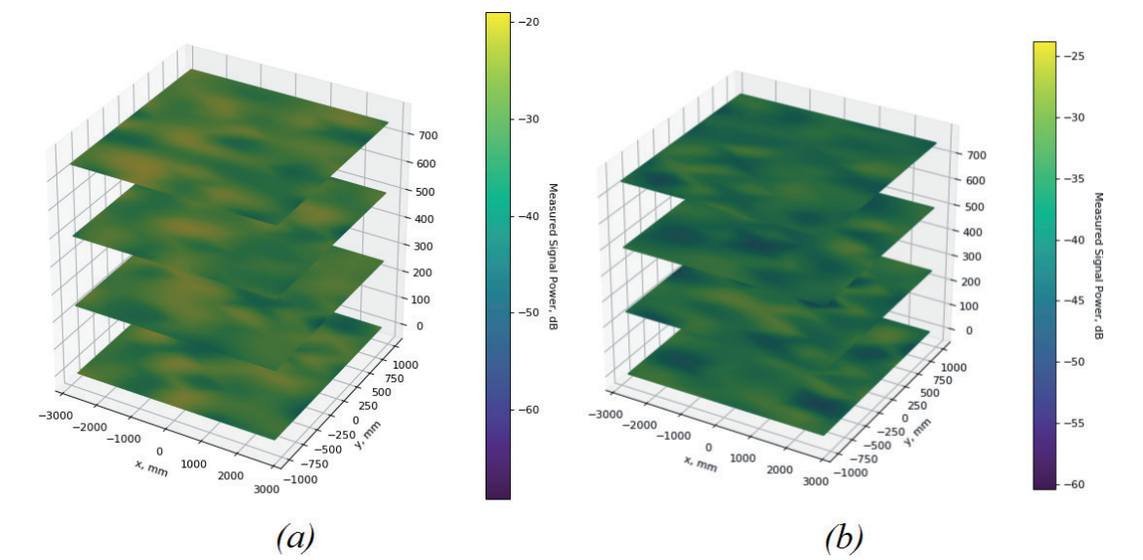

Figure 7.
3D interference map for (a) 868 MHz (LoRa) and (b) 2.484 GHz (Wi-Fi) for z = [0, 250, 500, 750], scenario **S3** *(three active transmitters).*

shift from the table's center to the sides. The only spectrum holes are present in the center of Scenario **S6** (**Figures 12** and **13**) at height z = 0 mm. However, they are very limited by the surrounding interference regions and are thus, hardly viable for the placement of communication nodes.

The same scenarios are illustrated for the Wi-Fi standard (**Figures 4**–**12**). They present more interesting results due to the higher carrier frequency, compared to LoRa. The strongest interference power is generally measured close to the transmitter, nevertheless, this does not hold for every scenario as is seen in **Figures 7** and **9**. Additionally, it is observed that the interfering signals dissipate more intensively in the higher elevation levels (500 and 750 mm) so that the sections with the highest power are shrinking while the medium (yellow/light green) and low (dark green/violet) regions are expanding (**Figure 8**). Thus, the increase in fading with distance both on the same plane but also with height in 3D is a significant factor in the 2.4 GHz ISM band. The interference sources' influence can be substantially diminished if their height is varied. As a consequence, drone-based and other mobile IoT devices can benefit from their abilities for repositioning in 3D.

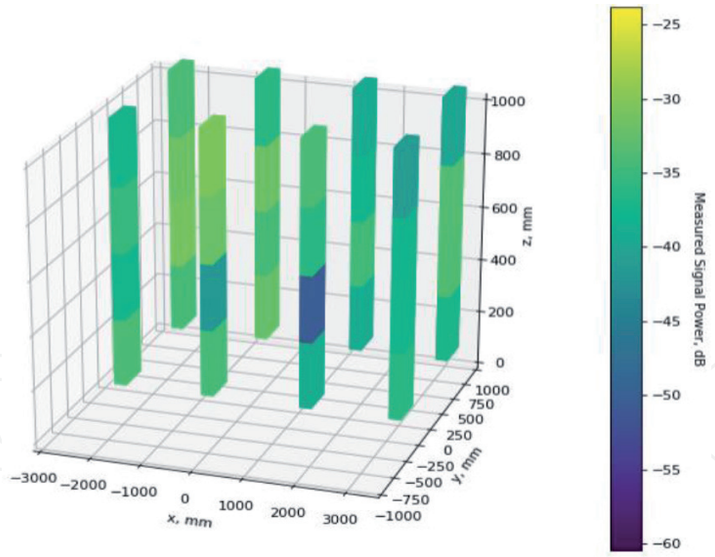

Figure 8.
3D bar plot for the Wi-Fi sensor standard, z = [0, 250, 500, 750] and x = [−2800, −1000, 1000, 2800], scenario **S3**.

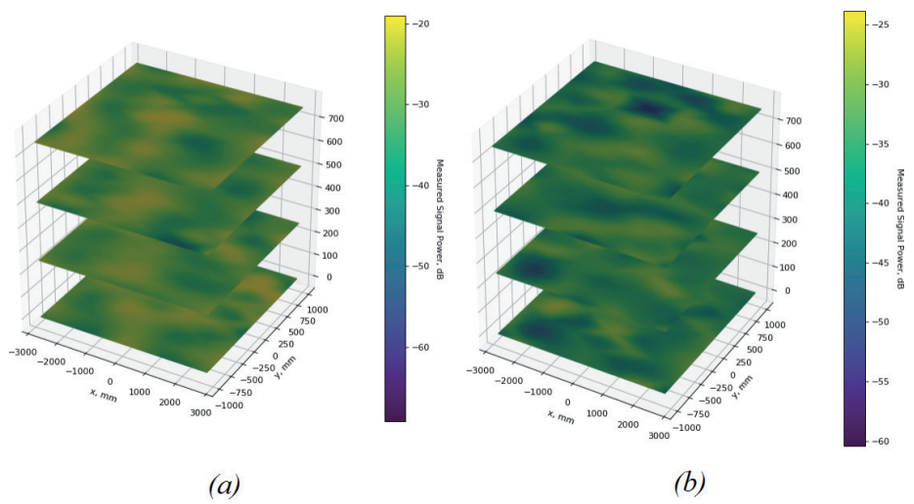

Figure 9.
3D interference map for (a) 868 MHz (LoRa) and (b) 2.484 GHz (Wi-Fi) for z = [0, 250, 500, 750], scenario **S4** *(four active transmitters, farthest position).*

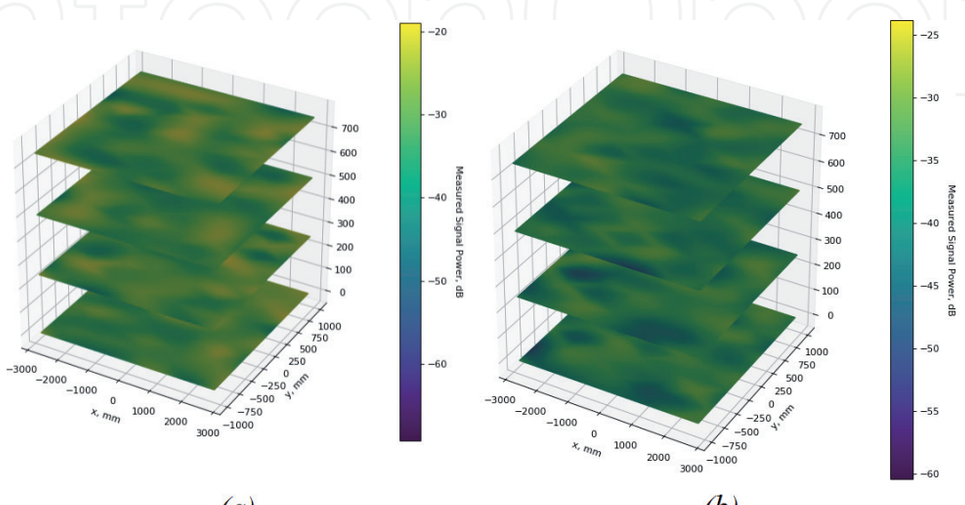

Figure 10.
3D interference map for (a) 868 MHz (LoRa) and (b) 2.484 GHz (Wi-Fi) for z = [0, 250, 500, 750], scenario **S5** *(four active transmitters, middle position).*

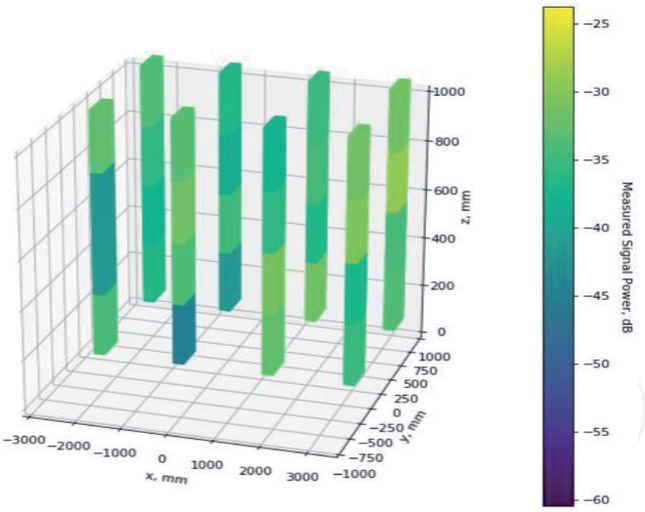

Figure 11.
3D bar plot for the Wi-Fi sensor standard, z = [0, 250, 500, 750] and x = [−2800, −1000, 1000, 2800], scenario **S5**.

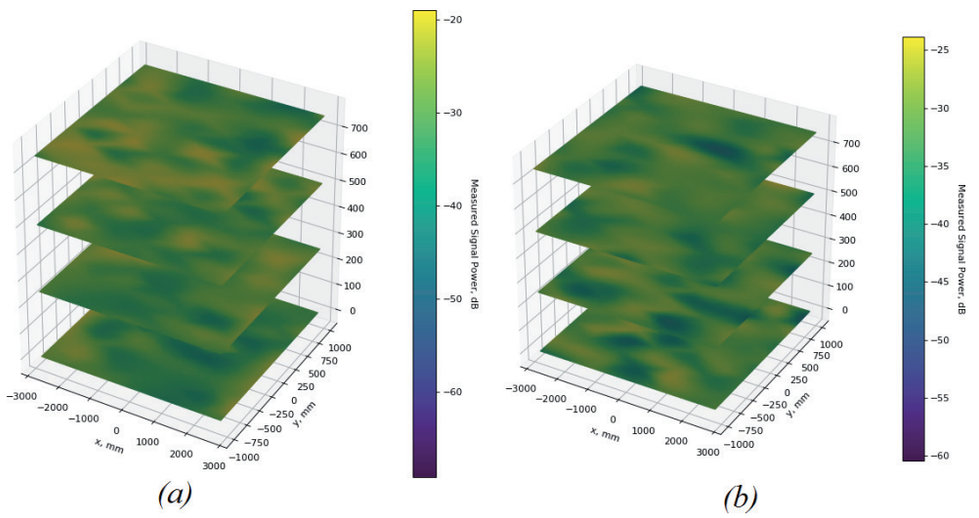

Figure 12.
3D interference map for (a) 868 MHz (LoRa) and (b) 2.484 GHz (Wi-Fi) for z = [0, 250, 500, 750], scenario **S6** *(four active transmitters, closest position).*

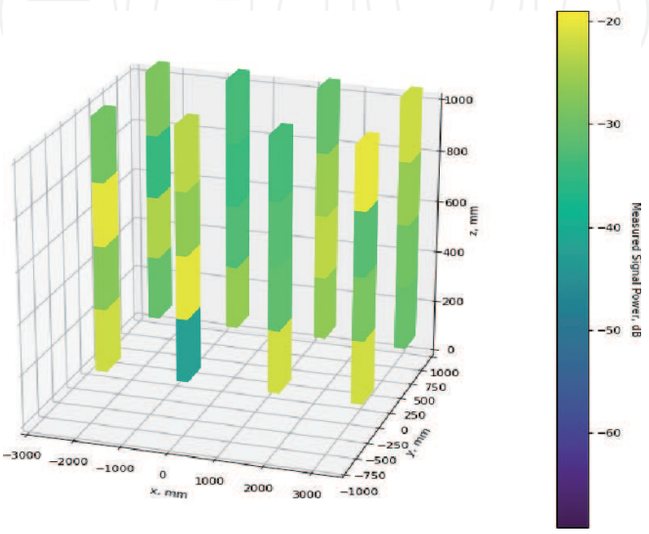

Figure 13.
3D bar plot for the LoRa sensor standard, z = [0, 250, 500, 750] and x = [−2800, −1000, 1000, 2800], scenario **S6**.

Figures	Value (mm)
6	[−2000, 0], [−2000, 1000], [0, 0], [0, 1000], [2000, 0], [2000, 1000]
9, 12, and 14	[−2800, 0], [−2800, 1000], [−1000, 0], [−1000, 1000], [1000, 0], [1000, 1000], [2800, 0], [2800, 1000]

Table 3.
Coordinates in x- and y-axes.

When it comes to scenarios **S5** and **S6**, there is some noticeable change in the interference distribution (**Figures 10–12**), as the spectrum holes shift to the table's center. At the same time, the interference power has increased substantially, mainly in the observed area's periphery. Thus, when the interferers are within a very short distance between each other, it is much more difficult to diminish their influence, even in the higher levels of elevation.

4. Conclusion

This chapter presents a spectrum occupancy evaluation for two popular IoT communication standards, LoRa and Wi-Fi, based on extensive experiments. These include the change of the interfering nodes' number and their location in dense indoor placement. The implementation is realized using the PlutoSDR hardware platform. The 3D interference maps show that the effect of fading with distance on the same plane and in height is crucial in localizing interference-free areas in dense deployments where even with the wireless standards' mechanisms for multiple accesses, it is likely that some nodes and/or malicious users will create in-band interference. In the case of LoRa in the 868 MHz band, interference is a much more substantial issue, regardless of the interferers' number and proximity. As for Wi-Fi sensors, due to the much higher carrier frequency, the interference's influence may be reduced substantially even within the span of a couple of meters. Thus, algorithms for adaptive repositioning in 3D have the potential for improving the communications of indoor IoT networks, aside from or in concurrency with future dynamic access techniques such as volumetric spectrum sensing [26]. Such methods can also be extended with Deep Learning-based node identification for protection against physical layer attacks [27].

Acknowledgements

This work was supported by project No D-098-2019 "Monitoring and analysis of the spectrum occupancy and interference in ISM ranges for the implementation of reliable IoT applications."

Author details

Antoni Ivanov*, Viktor Stoynov, Kliment Angelov, Radostin Stefanov, Dimitar Atamyan, Krasimir Tonchev and Vladimir Poulkov
Technical University of Sofia, Sofia, Bulgaria

*Address all correspondence to: astivanov@tu-sofia.bg

References

[1] Singh RP, Javaid M, Haleem A, Suman R. Internet of things (IoT) applications to fight against COVID-19 pandemic. Diabetes and Metabolic Syndrome: Clinical Research and Reviews. 2020;**14**:521-524

[2] Gubbi J, Buyya R, Marusic S, Palaniswami M. Internet of Things (IoT): A vision, architectural elements, and future directions. Future Generation Computer Systems. 2013;**29**(7):1645-1660

[3] Sarker VK, Queralta JP, Gia TN, Tenhunen H, Westerlund T. A survey on LoRa for IoT: Integrating edge computing. In: 2019 Fourth International Conference on Fog and Mobile Edge Computing (FMEC); 10 June 2019. IEEE. pp. 295-300

[4] ITU. Frequency Ranges for Global or Regional Harmonization of Short-Range Devices. Geneva: ITU-R, Radiocommunication; 2011

[5] Baccour N, Puccinelli D, Voigt T, Koubaa A, Noda C, Fotouhi H, et al. External radio interference. In: Radio Link Quality Estimation in Low-Power Wireless Networks. Heidelberg: Springer; 2013. pp. 21-63

[6] Centenaro M, Vangelista L, Zanella A, Zorzi M. Long-range communications in unlicensed bands: The rising stars in the IoT and smart city scenarios. IEEE Wireless Communications. 2016;**23**(5):60-67

[7] Patel D, Won M. Experimental study on low power wide area networks (LPWAN) for mobile Internet of Things. In: 2017 IEEE 85th Vehicular Technology Conference (VTC Spring); 4 June 2017. IEEE; 2017. pp. 1-5

[8] Ericsson A. Cellular Networks for Massive IoT—Enabling Low Power Wide Area Applications. 2016. pp. 1-3

[9] Reynders B, Meert W, Pollin S. Range and coexistence analysis of long range unlicensed communication. In: 2016 23rd International Conference on Telecommunications (ICT); 16 May 2016. IEEE; 2016. pp. 1-6

[10] Ratasuk R, Mangalvedhe N, Zhang Y, Robert M, Koskinen JP. Overview of narrowband IoT in LTE Rel-13. In: 2016 IEEE Conference on Standards for Communications and Networking (CSCN); 31 October 2016. IEEE; 2016. pp. 1-7

[11] Shi C, Liu J, Liu H, Chen Y. Smart user authentication through actuation of daily activities leveraging WiFi-enabled IoT. In: Proceedings of the 18th ACM International Symposium on Mobile Ad Hoc Networking and Computing; 10 July 2017. pp. 1-10

[12] Chi T, Chen M. A frequency hopping method for spatial RFID/WiFi/Bluetooth scheduling in agricultural IoT. Wireless Networks. 2019;**25**(2):805-817

[13] Pokhrel SR, Vu HL, Cricenti AL. Adaptive admission control for IoT applications in home WiFi networks. IEEE Transactions on Mobile Computing. 2019. DOI: 10.1109/TMC.2019.2935719

[14] Pirayesh H, Sangdeh PK, Zeng H. Coexistence of Wi-Fi and IoT communications in WLANs. IEEE Internet of Things Journal. 2020;**7**:7495-7505

[15] Sheth J, Dezfouli B. Enhancing the energy-efficiency and timeliness of IoT communication in WiFi networks. IEEE Internet of Things Journal. 2019;**6**(5):9085-9097

[16] Morse J. Market pulse: Wireless in industrial systems: Cautious enthusiasm. Industrial Embedded Systems. 2006;**2**(7):10-11

[17] OnWorld. WSN for Smart Industries: A Market Dynamics Report. 2007

[18] Gummadi R, Wetherall D, Greenstein B, Seshan S. Understanding and mitigating the impact of RF interference on 802.11 networks. ACM SIGCOMM Computer Communication Review. 2007;**37**(4):385-396

[19] Beltramelli L, Mahmood A, Gidlund M, Osterberg P, Jennehag U. Interference modelling in a multi-cell lora system. In: 2018 14th International Conference on Wireless and Mobile Computing, Networking and Communications (WiMob). IEEE; 2018. pp. 1-8

[20] Farhad A, Kim DH, Pyun JY. Scalability of LoRaWAN in an urban environment: A simulation study. In: 2019 Eleventh International Conference on Ubiquitous and Future Networks (ICUFN). IEEE; 2019. pp. 677-681

[21] Abbas R, Al-Sherbaz A, Bennecer A, Picton P. Collision evaluation in low power wide area networks. In: 2019 IEEE Smart-World, Ubiquitous Intelligence & Computing, Advanced & Trusted Computing, Scalable Computing & Communications, Cloud & Big Data Computing, Internet of People and Smart City Innovation (Smart-World/SCALCOM/UIC/ATC/CBDCom/IOP/SCI). IEEE; 2019. pp. 1505-1512

[22] Harrold T, Cepeda R, Beach M. Long-term measurements of spectrum occupancy characteristics. In: 2011 IEEE International Symposium on Dynamic Spectrum Access Networks(DySPAN). IEEE; 2011. pp. 83-89

[23] Analog Devices, Inc. ADALM-PLUTO—Software-Defined Radio Active Learning Module [Internet]. Available from: https://www.analog.com/en/design-center/evaluation-hardware-and-software/evaluation-boards-kits/adalm-pluto.html [Accessed: 21 July 2020]

[24] The GNU Radio Foundation. GNU Radio, the free and open software radio ecosystem [Internet]. Available from: http://gnuradio.org [Accessed: 21 July 2020]

[25] Urkowitz H. Energy detection of unknown deterministic signals. Proceedings of the IEEE. 1967;**55**(4):523-531

[26] Saad W, Bennis M, Chen M. A vision of 6G wireless systems: Applications, trends, technologies, and open research problems. IEEE Network. 2019;**34**:134-142

[27] Singh P, Pawar P, Trivedi A. Physical layer security approaches in 5g wireless communication networks. In: 2018 First International Conference on Secure Cyber Computing and Communication (ICSCCC). IEEE; 2018. pp. 477-482